Crystal Structure of *Klebsiella aerogenes* UreE, a Nickel-binding Metallochaperone for Urease Activation*

Hyun Kyu Song‡§, Scott B. Mulrooney¶, Robert Huber‡, and Robert P. Hausinger¶‖

From the ‡Abteilung Strukturforschung, Max-Planck-Institut für Biochemie, Am Klopferspitz 18a, D-82152, Planegg-Martinsried, Germany and the ¶Departments of Microbiology & Molecular Genetics and Biochemistry & Molecular Biology, Michigan State University, East Lansing, Michigan 48824

UreE is proposed to be a metallochaperone that delivers nickel ions to urease during activation of this bacterial virulence factor. Wild-type *Klebsiella aerogenes* UreE binds approximately six nickel ions per homodimer, whereas H144*UreE (a functional C-terminal truncated variant) was previously reported to bind two. We determined the structure of H144*UreE by multiwavelength anomalous diffraction and refined it to 1.5 Å resolution. The present structure reveals an Hsp40-like peptide-binding domain, an Atx1-like metal-binding domain, and a flexible C terminus. Three metal-binding sites per dimer, defined by structural analysis of Cu-H144*UreE, are on the opposite face of the Atx1-like domain than observed in the copper metallochaperone. One metal bridges the two subunits via the pair of His-96 residues, whereas the other two sites involve metal coordination by His-110 and His-112 within each subunit. In contrast to the copper metallochaperone mechanism involving thiol ligand exchanges between structurally similar chaperones and target proteins, we propose that the Hsp40-like module interacts with urease apoprotein and/or other urease accessory proteins, while the Atx1-like domain delivers histidyl-bound nickel to the urease active site.

Urease (EC 3.5.1.5) is a nickel-containing enzyme that catalyzes the hydrolysis of urea to produce ammonia and carbamate (1). Increased pH arising from this reaction is critical to the virulence of several human and animal pathogens (2). The crystal structure of urease from *Klebsiella aerogenes* provided the first three-dimensional model of the protein and revealed a unique dinuclear active site with the metal ions bridged by a carbamylated lysine residue (3, 4). Subsequent investigations of ureases from *Bacillus pasteurii* (5) and *Helicobacter pylori* (6) show essentially identical active site structures. Proper assembly of this metallocenter is a key step for maturation of urease and, in *K. aerogenes*, involves the products of the *ureD*,

ureE, *ureF*, and *ureG* accessory genes located adjacent to the structural genes (*ureA*, *ureB*, and *ureC*) (7). UreD, UreF, and UreG are known to form a series of complexes with urease apoprotein (8–11) and are suggested to act as a molecular chaperone for activation (7). *In vitro* activation and mutagenesis studies of the largest of these complexes, UreD-UreF-UreG-urease apoprotein (UreDFG-apourease), reveal that UreG functions as a GTPase during activation (12). Urease within the UreDFG-apourease complex can be fully activated in the presence of nickel, bicarbonate (for lysine carbamylation), GTP, and UreE (13). The latter protein is proposed to function as a "metallochaperone" by delivering nickel ions to UreDFG-apourease (14).

The metal-binding properties of wild-type UreE and H144*UreE, which has 15 residues truncated C-terminally, have been extensively characterized (15–18). The wild-type protein binds approximately six nickel ions per homodimer in distorted octahedral geometry with an average of three-five histidine donors per metal ion (14, 16). Most of these ligands are presumed to derive from the C-terminal fragment that contains 10 histidines within the last 15 residues. H144*UreE lacking the His-rich region is competent for activating urease *in vivo* (15) but was reported to bind only two nickel ions per dimer; thus, internal ligands, not the histidine residues at the C terminus, are necessary for UreE to assist in *K. aerogenes* urease activation (15). Based on extensive mutagenesis and spectroscopic studies of H144*UreE, a model for the critical nickel-binding sites was proposed (17). Structural information of UreE is desired to test the validity of this model and to identify potential residues involved in interaction with urease.

Major advances have been made in understanding the structure and function of copper metallochaperones in recent years (19, 20); however, structural information on chaperones for other metals is lacking. Here we provide the first view of a suspected metallochaperone for nickel incorporation. The H144*UreE structure reveals a unique two-domain architecture with one domain structurally related to a heat shock protein and the second to the Atx1 copper metallochaperone. Significantly, the metal-binding sites in UreE and Atx1 are distinct in location and types of residues despite the relationship between these proteins. In contrast to the thiol ligand exchange mechanism used by the copper metallochaperones (21, 22), we propose a distinct mechanism for UreE activation of urease.

§ Current address and to whom correspondence may be addressed: Dept. of Cancer Biology, Dana-Farber Cancer Inst. and Dept. of Molecular Pharmacology, Harvard Medical School, 44 Binney St., Boston, MA 02115; E-mail: hksong@red.dfci.harvard.edu.

‖ To whom correspondence may be addressed: Tel.: 517-353-9675; Fax: 517-353-8957; E-mail: hausinge@msu.edu.

EXPERIMENTAL PROCEDURES

Purification, Crystallization, and Data Collection—Recombinant H144*UreE and two of its variants (H91A and H110A) were purified as described previously (17), except that the host cells used were *Escherichia coli* B834(DE3). Protein was dialyzed against 20 mM Tris-HCl buffer, pH 7.5, containing 20 mM imidazole, 2 mM EDTA, and 2 mM dithiothreitol and then concentrated to 15 mg/ml. Crystallization was

TABLE I

Data collection and refinement statistics for H144*UreE variants

	H91A	H91A (+CuSO$_4$)[a]	H110A	H91A (MAD)		
				Remote	Edge	Peak
Data collection						
Wavelength (Å)	1.0500	1.0500	1.0500	0.9500	0.9815	0.9805
Resolution (Å)	1.5	2.5	2.8	1.95	1.95	1.95
(outer shell)[b]	(1.5–1.53)	(2.5–2.54)	(2.8–2.85)	(1.95–1.98)	(1.95–1.98)	(1.95–1.98)
Space group	P2$_1$	P2$_1$	P2$_1$2$_1$2$_1$	P2$_1$	P2$_1$	P2$_1$
Total reflections	633,762	198,257	76,825	438,425	432,989	438,552
Unique reflections	97,562	20,709	8,277	89,871	89,536	89,687
Completeness (%)[b]	96.9 (98.6)	97.5 (99.2)	98.5 (99.8)	98.7 (99.7)	98.7 (99.8)	98.8 (99.8)
R$_{merge}$ (%)[b,c]	2.6 (49.4)	4.8 (8.8)	8.7 (28.5)	3.0 (13.9)	2.8 (12.5)	3.6 (11.4)
Figure of merit[d] before/after DM				0.43 for 17–2.0 Å/0.66 for 17–1.5 Å		
Refinement						
Resolution range (Å)	17–1.5	17–2.5	17–2.8			
Number of reflections	91,545	20,352	8,021			
Number of reflections	91,545	20,352	8,021			
R$_{work}$/R$_{free}$ (%)[e]	22.3/26.1	22.3/29.5	23.7/31.8			
Number of atoms						
Protein	4,281	4,263	2,127			
Water/metal (Cu^{2+})	977/–	164/6	59/–			
r.m.s. bond length (Å)	0.005	0.007	0.007			
r.m.s. bond angles (°)	1.30	1.36	1.28			
Average B-value (Å^2)						
Main/side chain	22.5/26.6	46.6/48.2	49.9/50.3			
Water/metal (Cu^{2+})	41.7/–	43.1/52.2	36.0/–			

[a] Soaking in 50 mM CuSO$_4$ for 2 h.

[b] Values in parentheses are for reflections in the highest resolution bin.

[c] R$_{merge}$ = $\Sigma_h\Sigma_i|I(h,i) - \langle I(h)\rangle|/\Sigma_h\Sigma_i I(h,i)$, where I(h,i) is the intensity of the ith measurement of h and $\langle I(h)\rangle$ is the corresponding average value for all i measurements.

[d] Figure of merit = $|\Sigma P(\alpha)e^{i\alpha}/\Sigma P(\alpha)|$, where $P(\alpha)$ is the phase probability distribution and α is the phase.

[e] R$_{work}$ and R$_{free}$ = $\Sigma\|F_o| - |F_c\|/\Sigma|F_o|$ for the working set and test set (10%) of reflections.

performed by the hanging-drop vapor diffusion method at 22 °C. The reservoir solution for crystallization of the H91A mutant (native and Se-Met[1] substituted) consisted of 100 mM sodium cacodylate, pH 6.5, containing 18–19% (w/v) polyethylene glycol 8000 and 200 mM calcium acetate. For cryo-cooling, a crystal was transferred to reservoir solution containing 20% (v/v) glycerol before flash-freezing in a nitrogen stream at 100 K. The H91A mutant crystallized in the P2$_1$ space group with unit cell parameters of a = 43.88, b = 129.36, c = 56.79 Å, and β = 93.72°. The asymmetric unit contains four molecules of the polypeptide. The H110A mutant crystallized in a different form using slightly different crystallization conditions (100 mM sodium cacodylate, pH 6.5, 19–20% (w/v) polyethylene glycol 8000 and 200 mM magnesium acetate). The crystal belongs to the P2$_1$2$_1$2$_1$ space group with unit cell parameters of a = 40.11, b = 80.42, and c = 99.85 Å. The asymmetric unit contains a dimer. Due to a lack of reproducibility of the native crystals, the structure was determined by using multi-wavelength anomalous diffraction data collected from a crystal of the Se-Met-substituted H91A variant (Table I). Data were collected on a charge-coupled device detector at the BW6 beamline of the Deutsche Elektronen Synchrotron Center, Hamburg, Germany. Diffraction data were processed and scaled using the HKL software package (23).

Structure Determination and Refinement—Fifteen of 16 possible selenium sites (including four N-terminal methionine) in the H91A asymmetric unit were located with SOLVE (24). The phases were improved and extended to 1.5 Å with DM (25). The initial model was built using the warpNtrace option of the program ARP/warp (26) with the DM phase set as input. The model was rebuilt with the program O (27) using an electron density map based on the combination of the multiwavelength anomalous diffraction and model phases. The protein model was refined with CNS (28), including the bulk solvent correction. The 4-fold noncrystallographic symmetry was maintained with tight restraint during the early stages of refinement but was relaxed in the final rounds. The model of the H144*UreE (H91A) mutant (Se-Met substituted) accounts for 138 residues in three molecules and 140 residues in one molecule. No electron density was observed for the C-terminal segments (139–144). Solvent molecules were added using model-phased difference Fourier maps by using CNS (28). Statistics for the refined model are described in Table I. Subsequently, the structure of H144*UreE (H91A) complexed with Cu^{2+} ions was also refined (Table I). The positions of the metals were clearly determined by using model-phased difference Fourier map at 8 σ and confirmed by the

anomalous difference Fourier map. The initial phases of the H144*UreE (H110A) crystal were determined by the molecular replacement method using AmoRe (29). Refinement of the model was performed as above. The geometry of the models was assessed by the program PROCHECK (30), and the secondary structure elements were assigned by the program PROMOTIF (31). Coordinates of the Se-Met-substituted H144*UreE (H91A), this protein complexed with Cu^{2+}, and H144*UreE (H110A) have been deposited in the Protein Data Bank under ID codes 1gmu, 1gmw, and 1gmv, respectively.

RESULTS AND DISCUSSION

Overall Structure of UreE—The H144*UreE homodimer has an elongated shape with approximate dimensions of 90 × 43 × 32 Å (Fig. 1a). Each monomer folds into two discrete domains with approximate dimensions of 58 × 32 × 30 Å (Fig. 1b). The first domain (termed the peptide-binding domain; residues 1–70) consists of two β-sheets (A1, Leu-2-Leu-4; A2, Arg-29-Thr-33; A3, Asp-39-Leu-43; and B1, Gln-6-Arg-7; B2, Ala-16-Leu-20; B3, Val-55-Ser-57; B4, Phe-64-Ala-69) and a short α-helix (H1, Ile-22-Arg-25), while the second domain (termed the metal-binding domain; residues 71–133) consists of an antiparallel β-sheet (C1, Asp-71-Arg-78; C2, Gln-100-Met-102; C3, Glu-105-His-109; C4, Val-125-Pro-131) and two α-helices (H2, Pro-82-Asn-94; and H3, His-112-Arg-119). The C-terminal tail is flexible and would be followed by a characteristic histidine-rich segment (10 of the last 15 residues) in the wild-type UreE protein (15). A superposition of the four refined models (two crystal forms with dimers in the asymmetric unit) shows that the peptide-binding domain and the C terminus are flexible (Fig. 1c), consistent with the dramatic B-factor distribution of a monomer in the H110A structure (Fig. 1d). The average B-factors of the N- and C-domains in a monomer of this protein are 91.5 and 37.9 Å^2. A long α-helix (H2), a short β-strand (C2), their connecting loop, and a portion of C-terminal tail are involved in dimerization (Fig. 1a). For both crystal forms the dimer interface is composed of the following residues: Pro-82, Phe-83, Leu-85, Ala-86, Lys-87, Cys-89, Tyr-90, His-91, Gly-93, Asn-94, His-96, Val-97, Pro-98, Leu-99, Ile-101, Met-102, Pro-103, Glu-135, and Gly-137. The interface accessible surface

---

[1] The abbreviation used is: Se-Met, selenomethionine.
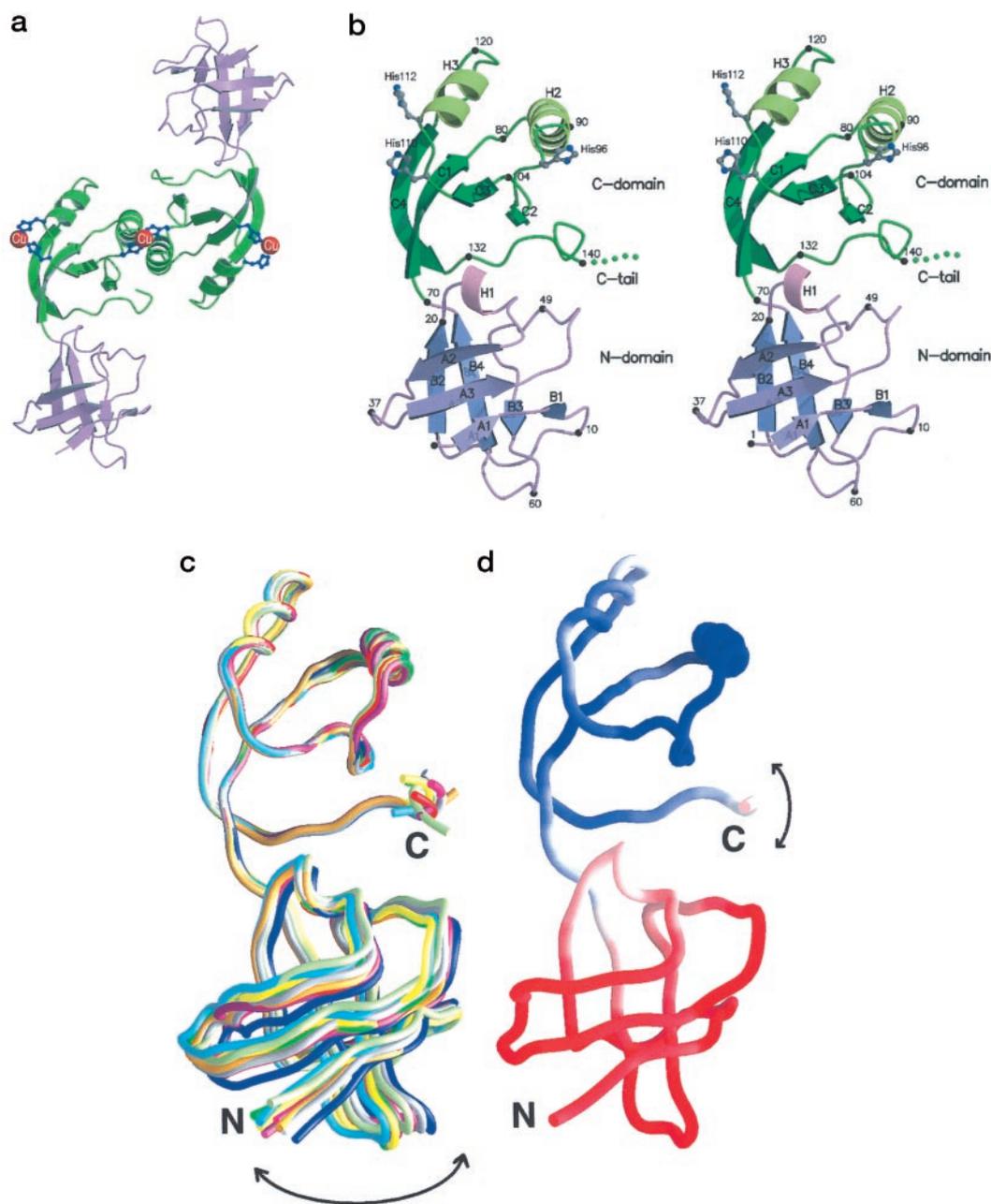
FIG. 1. **Structure of the *K. aerogenes* H144*UreE nickel metallochaperone.** *a,* ribbon diagram indicating the two-domain dimeric structure (the putative peptide-binding domain and the metal-binding domain are shown in *purple* and *green*, respectively) and Cu^{2+}-binding sites. *b,* stereo ribbon diagram showing the secondary structure elements of the metal-free monomer. Domains are colored as in *a*. Essential histidine residues (His-96, His-110, and His-112) for metal binding are shown and labeled. Approximately every tenth residue is also labeled and marked by a *black dot*. *c,* domain movement of the UreE monomer. Cα traces of UreE structures are drawn by overlapping their metal-binding domains (residues 71–132). *d,* temperature factor distribution of the UreE monomer. High temperature factors (flexible region) are *red* and low temperature factors (rigid region) are *blue*, ranging from 105.0 to 18.6 Å². Panels *a* and *b* were drawn with MOLSCRIPT (45) and rendered with RASTER 3D (46). Panels *c* and *d* were prepared with GRASP (47).

area is ~810 Å² per monomer (biochem.ucl.ac.uk/bsm/PP/server). This value is within the frequently observed range of the minimal buried surface area required for stable dimer association (32). This dimer interface is the most rigid part in the structure as shown in Fig. 1, *c* and *d*.

Peptide-binding Domain—Comparison to proteins in the DALI data base (33) indicated structural similarity (Z = 2.8) between the first domain of H144*UreE (residues 1–70) and the peptide-binding domain (domain I; residues 180–255) of yeast Hsp40 or Sis1 (34) (Fig. 2, *c* and *d*). A superposition of structurally equivalent residues in several secondary structural elements of UreE and the corresponding residues in Sis1 (PDB ID 1C3G) yields an r.m.s. deviation of 2.7 Å for 51

matching Cα atoms (UreE residues 15–32, 39–43, and 48–74). Many molecular chaperone/unfoldase proteins, including Hsp40, are known to utilize hydrophobic patches to form transient complexes with hydrophobic residues exposed in non-native peptides (35, 36). For example, domain I of Sis1 has a hydrophobic depression formed by residues Val-184, Leu-186, Ile-203, and Phe-251, and this was proposed as a binding site for interaction with non-native peptides (34). Intriguingly, UreE possesses a long hydrophobic canyon beginning in the putative peptide-binding domain (albeit at a different location that the hydrophobic region of Sis1) and extending into the metal-binding domain and C-terminal tail (Fig. 3*a*). In addition, many hydrophobic residues are located on the opposite
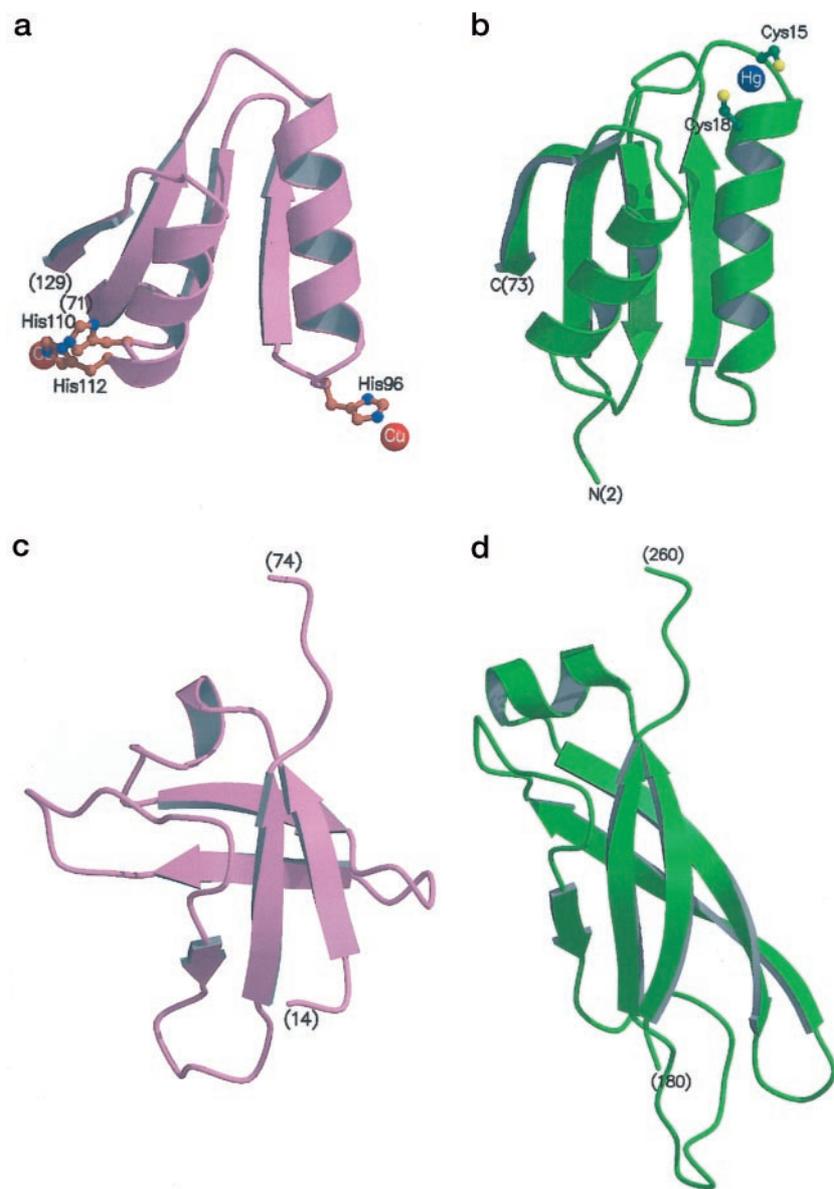
Fig. 2. **Structural homology of UreE domains to Atx1 and Sis1.** Ribbon diagrams are shown comparing the overall structures of the metal-binding domain of UreE *(a)*, Atx1 copper chaperone *(b)*, putative peptide-binding domain of UreE *(c)*, and domain I of Sis1 *(d)*. Metal-binding residues and bound metal ions are indicated (His-96, His-110, His-112, and Cu^{2+} in UreE; Cys-15, Cys-18, and Hg^{2+} in Atx1). Residues 1–13 and 130–138 in the UreE structure are not included for clarity.

surface of the suggested UreE peptide-binding domain (Fig. 3*c*). We presume that several of these residues are crucial for transient interaction of UreE with urease and/or the other accessory proteins, UreD, UreF, and UreG. The UreE variants examined thus far (Fig. 3, *b* and *d*) have focused on potential metal ligands (16, 17) and provide no insight into possible functions associated with these hydrophobic regions. As described above, the peptide-binding domain is not well ordered possibly as a consequence of lack of crystal packing. It may also be an intrinsic structural property (Fig. 1*d*) as expected for a module involved in transient protein-protein interactions. The illustrated conformation of UreE may differ from that when UreE interacts with its partners. Further biochemical and mutagenesis studies on this domain are needed to see whether this module has a peptide-binding role during urease activation.

Metal-binding Domain—When the complete three-dimensional structure of H144*UreE was compared with proteins in the DALI data base (33), a notable structural similarity (Z score > 2.0) was found in 89 proteins. Representatives showing the highest structural similarity are the pro-(activation) domain of procarboxypeptidase A2 (Z = 5.5), copper metallochaperone Atx1 (Z = 5.4), elongation factor G (Z = 5.2), the fourth metal-binding domain of Menkes copper-transporting ATPase

(Z = 5.1), and domain 1 of the copper chaperone for superoxide dismutase (Z = 4.5). The Atx1-like folding unit of these proteins shares an identical topology with the metal-binding domain of UreE (Fig. 2, *a* and *b*). The putative nickel metallochaperone metal-binding domain is very similar in overall structure to Atx1 despite a lack of overall sequence similarity (37). Superpositioning of structurally equivalent residues in several secondary structural elements of UreE and Atx1 (PDB ID 1CC8) yields an r.m.s. deviation of 1.9 Å for 50 matching Cα atoms (UreE residues 75–96, 98–109, 111–122, and 126–129, excluding parts that show large deviations). Despite sharing a common folding pattern, a significant structural difference exists between the metal-binding domain of UreE and Atx1. Specifically, Atx1 is known to be a monomer in solution (21), whereas UreE is a dimer in the presence or absence of nickel ions (14). The human homologue of Atx1 is a homodimer, but the intersubunit contacts for Hah1 (22) differ from that observed in UreE. Further studies involving mutagenesis and biophysical analysis are necessary to better understand the possible role of subunit interactions in the catalytic function of the UreE urease accessory protein.

Metal-binding Sites—Efforts to crystallize H144*UreE in the presence of nickel ions were not successful and addition of

nickel ions to preformed crystals led to their dissolution. These results parallel the reported inability to crystallize full-length wild-type UreE with nickel and the fracturing of wild-type apoprotein crystals upon nickel addition (14). As an alternative to obtaining the nickel-bound structure, we solved the copper-bound form of H144*UreE for which the metal binding properties are well characterized (17, 18). After soaking 50 mM CuSO$_4$
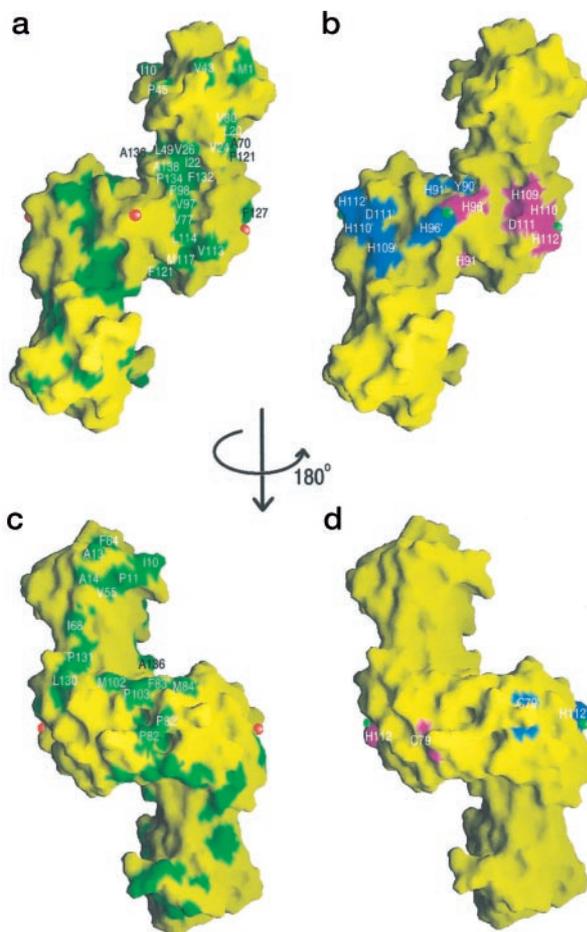
FIG. 3. **Surface representations of H144*UreE.** *a* and *c,* residues forming the hydrophobic surfaces of UreE are colored *green* and labeled. Bound-copper ions are shown as *red balls*. *b* and *d,* residues that have previously been subjected to mutagenesis are colored *magenta* and labeled in one subunit, and those in the other are colored *blue* and labeled with a prime (′). Bound-copper ions are shown as *green balls*. The view in *a* and *b* is the same as that in Fig. 1*a*, and the view in *c* and *d* is obtained by a 180° rotation around a vertical axis. Figs. were drawn with GRASP (47).

solution into pre-grown UreE crystals for 2 h, the copper-binding sites were readily located in the $(F_o - F_c)$ difference Fourier and anomalous difference maps (Fig. 4). The UreE dimer binds three copper ions (Fig. 1*a*), consistent with the reported three sequential Cu^{2+} binding steps observed by kinetics (18). The pair of His-96 residues binds one copper atom between the subunits, whereas the other two copper sites involve His-110 and His-112 from within each subunit (Fig. 4). These are the same three pairs of residues implicated by mutagenesis studies in nickel ion binding (17); however, equilibrium dialysis measurements have consistently shown only two nickel ions bound per H144*UreE (15, 17). We suggest that aberrant reactivity of UreE with protein assay reagents may have resulted in an underestimation of nickel binding by this protein. Significantly, only His-96 is conserved in all reported UreE sequences (17). As shown in Fig. 4, there is little conformational change in the main-chain between free and copper-complexed states (an r.m.s. deviation of less than 1.0 Å including the C-terminal tail) except for a dramatic side chain movement of His-112. Several water molecules (one or two for each binding site) also coordinate Cu^{2+}, but their relative positions differ as shown in Fig. 4.

Spectroscopic studies had earlier revealed a thiolate-to-Cu^{2+} charge-transfer transition in Cu^{2+}-bound H144*UreE that was absent in the C79A variant (17). Based on these results, some of us had concluded that one Cu^{2+} site must bind Cys-79. In contrast, we detect no additional electron density near residue Cys-79 in the structure, and this position is quite distant from the experimentally determined Cu^{2+}-sites (Fig. 3*d*). We suggest that the apparent discrepancy arises from comparison of solution studies *versus* investigation of Cu^{2+} addition to crystals. Specifically, we propose that in solution Cys-79 of one dimer interacts with a copper site in another dimer, whereas crystal packing prevents this interaction in the solid state. Perhaps related to such a proposed aggregation event, we observe transient turbidity upon adding copper ions to H144*UreE solutions. Selective binding of Hg^{2+} to Cys-79 (along with Met-84) supports the proposal that this residue is accessible for metal binding (data not shown). Intriguingly, Cys-79 of UreE is structurally equivalent to the metal-binding Cys-15 of Atx1; thus, further highlighting the relationship between these proteins (Fig. 2, *a* and *b*). While the Atx1 thiol is one of two cysteines essential to its copper metallochaperone role, Cys-79 is not important to function of UreE (17, 18). Cys-89, located in helix H2, has no counterpart in Atx1 and is not available to bind metals because it is involved in subunit dimerization.

Proposed Mechanism—While the structures of ureases from different sources (3, 5, 6) have provided details of the nickel-

FIG. 4. $F_o - F_c$ **electron density map of the metal-binding sites in His144*UreE.** *a,* the copper-binding site involving the pair of His-96 residues. *b,* the copper-binding sites involving His-110 and His-112. The maps were calculated using 17–2.5 Å data and contoured at 6 σ. The *blue* and *green* copper atoms and the different colored ribbons represent the superimposed molecules in the asymmetric unit. The distances indicated are an average value for the superimposed molecules in the crystallographic asymmetric unit. *Green* and *white* side-chains represent Cu^{2+}-complexed and free UreE, respectively. The positions of water molecules (*red balls*) differ in the four molecules. The figure was drawn with BOBSCRIPT (48) and rendered with RASTER 3D (46).

K. aerogenes UreE Crystal Structure

binding site and possible mechanisms of urea hydrolysis (1), our understanding of how nickel is incorporated into the enzyme is very limited. Assembly of the dinuclear nickel center requires that the pre-organized apoprotein structure (38) be partially opened up to expose the deeply buried metal-binding sites. This process, along with carbamylation of a specific lysine residue, appears to be carried out by a GTP-dependent molecular chaperone comprised of UreD, UreF, and UreG that forms the UreDFG-apourease complex (7). The role of nucleotide hydrolysis in urease activation remains unclear, but we speculate that it provides energy for conformational transitions like in the classical chaperone action (35, 36). The putative metallochaperone UreE participates in urease activation by delivering nickel ions but may also function in the molecular chaperone process. In particular, the putative peptide-binding domain of UreE that shares very similar architecture to Sis1 domain I may bind to urease apoprotein or an accessory protein to control specific conformational changes needed for activation. Conformational changes within UreE or the UreDFG-apourease may be coupled to nickel transfer from the proposed metallochaperone to the urease apoprotein, perhaps via His-96. We speculate that nickel ions are delivered one at a time to form the dinuclear site in urease, perhaps with the His-110/His-112 sites acting as a nickel reservoir to facilitate that process. Notably, this mechanism is unrelated to the thiol ligand exchange reactions that occur during copper delivery by copper metallochaperones (21, 22). It is also unrelated to the mechanism of iron sulfur cluster assembly mediated by NifS (39).

UreE has counterparts involved in the activation of two other nickel-containing enzymes (40), carbon monoxide dehydrogenase (41) and hydrogenase (42). CooJ of *Rhodospirillum rubrum* contains a C-terminal His-rich region and binds ~4 Ni^{2+} per monomer for incorporation into CO dehydrogenase (43). HypB from *Bradyrhizobium japonicum* possesses a His-rich sequence at the N terminus, binds 18 Ni^{2+} per dimer, and is proposed to have a dual role of both storing and delivering the metal to apohydrogenase (44). It is reasonable to suspect that CooJ and HypB perform similar roles with their target enzymes as UreE does in urease activation. Therefore, this structural study of UreE may provide more general insight into mechanisms of nickel enzyme activation.

REFERENCES

1. Hausinger, R. P., and Karplus, P. A. (2001) in *Handbook of Metalloproteins* (Wieghardt, K., Huber, R., Poulos, T. L., and Messerschmidt, A., eds), pp. 867–879, John Wiley & Sons, Ltd., West Sussex, UK
2. Mobley, H. L., Island, M. D., and Hausinger, R. P. (1995) *Microbiol. Rev.* **59,** 451–480
3. Jabri, E., Carr, M. B., Hausinger, R. P., and Karplus, P. A. (1995) *Science* **268,** 998–1004
4. Pearson, M. A., Michel, L. O., Hausinger, R. P., and Karplus, P. A. (1997) *Biochemistry* **36,** 8164–8172
5. Benini, S., Rypniewski, W. R., Wilson, K. S., Miletti, S., Ciurli, S., and Mangani, S. (1999) *Structure* **7,** 205–216
6. Ha, N. C., Oh, S. T., Sung, J. Y., Cha, K. A., Lee, M. H., and Oh, B. H. (2001) *Nat. Struct. Biol.* **8,** 505–509
7. Hausinger, R. P., Colpas, G. J., and Soriano, A. (2001) *ASM News* **67,** 78–84
8. Park, I. S., Carr, M. B., and Hausinger, R. P. (1994) *Proc. Natl. Acad. Sci. U. S. A.* **91,** 3233–3237
9. Park, I. S., and Hausinger, R. P. (1995) *J. Bacteriol.* **177,** 1947–1951
10. Moncrief, M. B., and Hausinger, R. P. (1996) *J. Bacteriol.* **178,** 5417–5421
11. Moncrief, M. B., and Hausinger, R. P. (1997) *J. Bacteriol.* **179,** 4081–4086
12. Soriano, A., and Hausinger, R. P. (1999) *Proc. Natl. Acad. Sci. U. S. A.* **96,** 11140–11144
13. Soriano, A., Colpas, G. J., and Hausinger, R. P. (2000) *Biochemistry* **39,** 12435–12440
14. Lee, M. H., Pankratz, H. S., Wang, S., Scott, R. A., Finnegan, M. G., Johnson, M. K., Ippolito, J. A., Christianson, D. W., and Hausinger, R. P. (1993) *Protein Sci.* **2,** 1042–1052
15. Brayman, T. G., and Hausinger, R. P. (1996) *J. Bacteriol.* **178,** 5410–5416
16. Colpas, G. J., Brayman, T. G., McCracken, J., Pressler, M. A., Babcock, G. T., Ming, L. J., Colangelo, C. M., Scott, R. A., and Hausinger, R. P. (1998) *J. Biol. Inorg. Chem.* **3,** 150–160
17. Colpas, G. J., Brayman, T. G., Ming, L. J., and Hausinger, R. P. (1999) *Biochemistry* **38,** 4078–4088
18. Colpas, G. J., and Hausinger, R. P. (2000) *J. Biol. Chem.* **275,** 10731–10737
19. Rosenzweig, A. C. (2001) *Acc. Chem. Res.* **34,** 119–128
20. O'Halloran, T. V., and Culotta, V. C. (2000) *J. Biol. Chem.* **275,** 25057–25060
21. Pufahl, R. A., Singer, C. P., Peariso, K. L., Lin, S. J., Schmidt, P. J., Fahrni, C. J., Culotta, V. C., Penner-Hahn, J. E., and O'Halloran, T. V. (1997) *Science* **278,** 853–856
22. Wernimont, A. K., Huffman, D. L., Lamb, A. L., O'Halloran, T. V., and Rosenzweig, A. C. (2000) *Nat. Struct. Biol.* **7,** 766–771
23. Minor, W., Tomchick, D., and Otwinowski, Z. (2000) *Structure* **8,** R105–R110
24. Terwilliger, T. C., and Berendzen, J. (1999) *Acta Crystallogr. Sect. D Biol. Crystallogr.* **55,** 849–861
25. *Collaborative Computational Project No. 4.* (1994) *Acta Crystallog. Sect. D Biol. Crystallogr.* **50,** 760–763
26. Perrakis, A., Morris, R., and Lamzin, V. S. (1999) *Nat. Struct. Biol.* **6,** 458–463
27. Jones, T. A., Zou, J.-Y., Cowan, S. W., and Kjeldgaard, M. (1991) *Acta Crystallogr. Sect. A* **47,** 110–119
28. Brünger, A. T., Adams, P. D., Clore, G. M., DeLano, W. L., Gros, P., Grosse-Kunstleve, R. W., Jiang, J. S., Kuszewski, J., Nilges, M., Pannu, N. S., Read, R. J., Rice, L. M., Simonson, T., and Warren, G. L. (1998) *Acta Crystallogr. Sect. D Biol. Crystallogr.* **54,** 905–921
29. Navaza, J. (1994) *Acta Cryst. Sect. A* **50,** 157–163
30. Laskowski, R., MacArthur, M., Hutchinson, E., and Thornton, J. (1993) *J. Appl. Crystallogr.* **26,** 283–291
31. Hutchinson, E. G., and Thornton, J. M. (1996) *Protein Sci.* **5,** 212–220
32. Jones, S., and Thornton, J. M. (1996) *Proc. Natl. Acad. Sci. U. S. A.* **93,** 13–20
33. Holm, L., and Sander, C. (1993) *J. Mol. Biol.* **233,** 123–138
34. Sha, B., Lee, S., and Cyr, D. M. (2000) *Structure* **8,** 799–807
35. Bukau, B., and Horwich, A. L. (1998) *Cell* **92,** 351–366
36. Hartl, F. U. (1996) *Nature* **381,** 571–579
37. Rosenzweig, A. C., Huffman, D. L., Hou, M. Y., Wernimont, A. K., Pufahl, R. A., and O'Halloran, T. V. (1999) *Structure* **7,** 605–617
38. Jabri, E., and Karplus, P. A. (1996) *Biochemistry* **35,** 10616–10626
39. Kaiser, J. T., Clausen, T., Bourenkow, G. P., Steinbacher, S., and Huber, R. (2000) *J. Mol. Biol.* **297,** 451–464
40. Watt, R. K., and Ludden, P. W. (1999) *Cell. Mol. Life Sci.* **56,** 604–625
41. Dobbek, H., Svetlitchnyi, V., Gremer, L., Huber, R., and Meyer, O. (2001) *Science* **293,** 1281–1285
42. Volbeda, A., Charon, M.-H., Piras, C., Hatchikian, E. C., Frey, M., and Fontecilla-Camps, J. C. (1995) *Nature* **373,** 580–587
43. Watt, R. K., and Ludden, P. W. (1998) *J. Biol. Chem.* **273,** 10019–10025
44. Olson, J. W., and Maier, R. J. (2000) *J. Bacteriol.* **182,** 1702–1705
45. Kraulis, P. J. (1991) *J. Appl. Crystallogr.* **24,** 946–950
46. Merritt, E. A., and Bacon, D. J. (1997) *Methods Enzymol.* **277,** 505–524
47. Nicholls, A., Bharadwaj, R., and Honig, B. (1993) *Biophys. J.* **64,** 166 (abstr.)
48. Esnouf, R. M. (1999) *Acta Crystallogr. Sect. D Biol. Crystallogr.* **55,** 938–940

Crystal Structure of *Klebsiella aerogenes* UreE, a Nickel-binding Metallochaperone for Urease Activation

Hyun Kyu Song, Scott B. Mulrooney, Robert Huber and Robert P. Hausinger

Access the most updated version of this article at doi: 10.1074/jbc.M108619200

Alerts:
- When this article is cited
- When a correction for this article is posted

Click here to choose from all of JBC's e-mail alerts

This article cites 47 references, 15 of which can be accessed free at
http://www.jbc.org/content/276/52/49359.full.html#ref-list-1